Definition of a methodology for local reduction of parallaxes in directly oriented images

V. Casella* - M. Franzini**

(*) DIET – University of Pavia – vittorio.casella@unipv.it
(**) DIET – University of Pavia – marica.franzini@unipv.it

Keywords: Direct photogrammetry, direct sensor orientation, residual parallaxes, stereoscopy.

1. Abstract

The paper concerns a procedure called Local Parallax Reduction, LPR. It could be useful during manual map compilation of directly oriented images, which sometimes present quite high values of residual parallaxes, because they may disturb optimal stereovision.

In the case that accuracies guaranteed by directly measured exterior orientation (EO from now) parameters are satisfactory, it is possible to perform an adjustment whose observations are the measurements of a sufficient number of tie points and the original EO parameters. The paper shows that, giving the right weights to the observations, a new set of EO values can be determined, such that parallaxes are greatly reduced, while accuracies remain substantially unchanged.

LPR can be applied to digital photogrammetric workstations as well as to analytical stereoplotters.

2. Introduction

It is known that aerial images which have been directly oriented with an integrated GPS-IMU sensor sometimes show non-negligible residual parallaxes. Even if the stereoplotted coordinates are generally adequately close to their true values, quality of stereovision is not always sufficient for the human operator. When such images are used for map compilation, the problem arises of how to reduce parallaxes.

This phenomenon is new for photogrammetry and its origin is easily recognized. Slightly widening its traditional meaning, we will use the expression *relative orientation* for blocks of images, indicating how well homologous rays intersect. We will also use the expression *absolute orientation* to indicate how close stereoplotted coordinates are to their true values.

In pre-inertial photogrammetry, aerial triangulation (AT in the following) is used to orient the images and different kinds of observations contribute to relative and absolute orientation. We will call them *relative orientation data* and *absolute orientation data*, respectively. The former is constituted by tie points, whose measure is easy and inexpensive, in both analytical and digital photogrammetry. The latter is composed of GCPs, measured on the ground, or positions of the camera centres, measured by means of kinematic GPS; it is more expensive and more risky, from the quality point of view.

As relative orientation data is easy to acquire, many measurements are usually taken, and photogrammetric blocks oriented with AT have in general a very good relative orientation. On the contrary, it may happen that absolute orientation is not brilliant, due to poor measurement of GCPs or to a disturbed GPS signal. Therefore, if the AT is performed with standard quality levels, the human operator will very seldom notice residual parallaxes great enough to disturb stereovision.

The usage of integrated inertial sensors radically changes things. If direct sensor orientation is performed, each image is orientated independently. Absolute orientation is quite accurate, in general, but relative orientation is weak, quite often, because of the *absolute lack of relative orientation data*.

Several solutions are possible. One is integrated sensor orientation, which requires performing an AT calculation. Some companies perform a type of integrated sensor orientation, that could be called *light integrated*, because they only use, as observations, automatically measured tie points and the exterior orientations given by the sensor. No GCPs are inserted, which is different from the proper integrated procedure.

But there are some good arguments against the usage of AT with direct photogrammetry. Some people think that there is a contradiction in terms between AT and direct photogrammetry. If the adjustment is still needed, there is a

much cheaper solution constituted by AAT and GPS measurements of camera centres. We don't think this is a definitive argument, but it is certainly a good observation.

Besides this, the solution of light integrated orientation is operationally convenient only if digital images are available. But if the workflow is based on analogue images, and we know there are many analytical stereoplotters working in the world, it becomes heavy because there are two possibilities to obtain EO parameter optimization: to perform a manual analytical triangulation on analogue images or to digitize them. They are both unsatisfactory.

For all these reasons we think that a procedure of Local Parallax Reduction (LPR) is useful, purely working on single models, where the term *local* comes from. The procedure we conceived doesn't require any additional data except the image coordinates of a sufficient number of tie points; they could be measured manually or automatically, indifferently. By adjusting these image coordinates, together with the original EO data, and assigning right weights to them, a new set of EO values can be determined. They are slightly changed from the original ones, such that parallaxes are greatly reduced, while accuracies remain substantially unchanged.

From the operational point of view we imagine that the operator, once he has noticed that a couple shows fastidious parallaxes, starts a procedure that allows him to collimate a certain number of well distributed tie points. Then LPR is performed and new EO values are determined and used. The operator can collimate new points as required, as he usually does during the relative orientation calculation, until he reaches good results.

LPR needn't be applied to all models, but only to those which show non negligible parallaxes, under the operator's judgment. Such a procedure could be easily inserted into DPWs as well as into the less recent analytical stereoplotters, which are still often used for map production.

3. The dataset

To approach the problem described above, we considered a rectangular **block** constituted by 3 strips and 8 images per strip. The block was acquired over Pavia's test site in year 2000 by a plane of the Compagnia Generale Ripreseaeree – CGR equipped with a Leica RC30 **camera**, provided with an Applanix POS/AV 510 sensor. The focal length of the lens was 300 mm; the average relative height of the flight was 2900 m; the average image scale, 1:9300. The **digital images** we used were acquired by a Zeiss SCAI scanner with a resolution of 14 microns per pixel.

For that flight the **exterior orientation data** obtained with a calibration process of the type direct sensor orientation is available. Calibration was performed by the CGR company with the standard Applanix software.

In the block's area there are 56 natural **GCPs** which were measured with high quality GPS surveying. Besides this, we chose at least 18 **tie points** per image, corresponding to 2 points for each of the 9 canonical positions in the model.

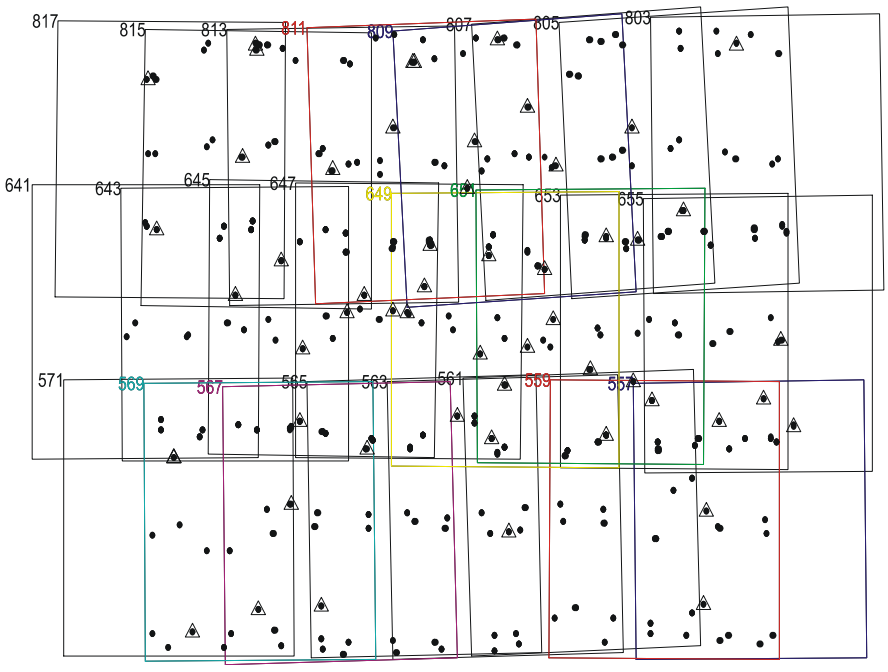

Figure 1 – Overview of the dataset: 24 images, 56 GCPs represented by triangles, 209 tie points represented by black dots. Coloured images are used for testing the LPR procedure.

All the GCPs and tie points were measured in all the images in which they are visible. We performed these measurements with a Socet Set DPW, in the monoscopic mode. We used Socet Set only for measuring image coordinates, because all the following processing has been carried out with proprietary scientific software developed in the Matlab environment.

Precision of image coordinate measurements was investigated. Six points were chosen, representing the various quality levels in terms of sharpness and visibility, and they were repeatedly measured 10 times by an operator and again 10 times by another one. Results are summarized in Table 1, which shows that the worst std is around 4 microns.

Point name	Image name	Repetitions	Std X (μm)	Std Y (μm)
TP_5_653_99	7_559	20	2.1	1.3
	7_557	20	1.5	1.5
TP_7_559_99	7_559	20	2.4	2.7
	7_557	20	2.6	5.0
TP_7_561_5	7_559	20	1.9	1.7
	7_557	20	3.9	3.2
TP_5_643_99	7_559	20	2.8	2.5
	7_557	20	2.0	2.2
TP_7_569_5	7_559	20	1.6	1.2
	7_557	20	1.6	1.7
TP_7_571_9	7_559	20	2.3	3.0
	7_557	20	1.9	3.5

Table 1 – Summary of precision of monoscopic measurements of image coordinates.

Among all the canonical models, characterized by having the base along the X axis and the along-track overlap of 60%, we chose four characterized by high parallax values and the presence of a good number of GCPs. They are drawn in colour mode in Figure 1. We will refer to these four models as the LPR dataset.

4. The adopted method for parallaxes estimation

The term *parallax* is related to the fact that, due to many reasons, homologous rays don't really intersect. This affects the precision of measurements and also has well known effects on the quality of manual stereoplotting, because the human operator sees the measuring marks doubled and loses the stereovision, if the parallaxes are above a certain threshold.

Despite the fact that the term *parallax* is often used as if it were well and uniquely defined, literature presents many ways of measuring the non-intersection of rays, therefore there are many ways of defining and measuring the parallax, even if they are all related to the same phenomenon. Some are based on traditional relative orientation formulas, and many choices are possible within this frame. Another approach relies on direct characterization, in terms of vector calculus, of the coplanarity condition. A different method is used when the AT is performed: parallaxes are estimated through the residuals between the measured image coordinates and the estimated ones. The latter manner obviously requires the AT calculation, otherwise it only applies to points whose object coordinates are known.

All these methods give results which are convertible, but aren't easily and directly comparable. Therefore we looked for a way of measuring the parallax with the following characteristics: (i) easily applicable to directly oriented images; (ii) having a clear definition and simple meaning; (iii) showing a direct coupling with the operators' observation. We decided to estimate the parallax in the object space by means of well known formulas which are illustrated in the following. Considering a stereocouple, an object-point P, whose object-coordinates are (X_P, Y_P, Z_P), and its image-points π_1 and π_2, belonging to the two images, whose image-coordinates are respectively $(x^{(1)}, y^{(1)})$ and $(x^{(2)}, y^{(2)})$, four equations can be deduced from the collinearity equations

$$
\begin{aligned}
X_P &= X_0^{(1)} + \left(Z_P - Z_0^{(1)}\right) K_x^{(1)} \qquad & K_x^{(1)} &= \frac{R_{11}^{(1)}\, x^{(1)} + R_{12}^{(1)}\, y^{(1)} R_{13}^{(1)}\, c}{R_{31}^{(1)}\, x^{(1)} + R_{32}^{(1)}\, y^{(1)} - R_{33}^{(1)}\, c} \\
Y_P &= Y_0^{(1)} + \left(Z_P - Z_0^{(1)}\right) K_y^{(1)} \qquad & K_y^{(1)} &= \frac{R_{21}^{(1)}\, x^{(1)} + R_{22}^{(1)}\, y^{(1)} R_{23}^{(1)}\, c}{R_{31}^{(1)}\, x^{(1)} + R_{32}^{(1)}\, y^{(1)} - R_{33}^{(1)}\, c} \\
X_P &= X_0^{(2)} + \left(Z_P - Z_0^{(2)}\right) K_x^{(2)} \qquad & K_x^{(2)} &= \frac{R_{11}^{(2)}\, x^{(2)} + R_{12}^{(2)}\, y^{(1)} R_{13}^{(2)}\, c}{R_{31}^{(2)}\, x^{(2)} + R_{32}^{(2)}\, y^{(2)} - R_{33}^{(2)}\, c} \\
Y_P &= Y_0^{(2)} + \left(Z_P - Z_0^{(2)}\right) K_y^{(2)} \qquad & K_y^{(2)} &= \frac{R_{21}^{(2)}\, x^{(2)} + R_{22}^{(2)}\, y^{(2)} R_{23}^{(2)}\, c}{R_{31}^{(2)}\, x^{(2)} + R_{32}^{(2)}\, y^{(2)} - R_{33}^{(2)}\, c}
\end{aligned}
\tag{1}
$$

The first couple represents a line in the space, which is defined by points π_1 and $\boldsymbol{X}_0^{(1)}$ (the perspective centre of image 1). The second couple represents another line, defined by π_2 and $\boldsymbol{X}_0^{(2)}$. Under the hypothesis that the two lines are not parallel and that the *X* component of the base $\boldsymbol{X}_0^{(2)} - \boldsymbol{X}_0^{(1)}$ is prevailing, the following solution is feasible. The two lines are projected into the *X*-*Z* space, where they necessarily intersect. The *X* and *Z* coordinates of the *P* point are thus obtained. Formally, this is equivalent to solve the subsystem constituted by equations #1 and #3:

$$
\begin{aligned}
X_P &= X_0^{(1)} + \frac{X_0^{(2)} - X_0^{(1)} - Z_0^{(2)} K_x^{(2)} + Z_0^{(2)} K_x^{(2)}}{K_x^{(1)} - K_x^{(2)}} K_x^{(1)} \\
Z_P &= \frac{X_0^{(2)} - X_0^{(1)} - Z_0^{(2)} K_x^{(2)} + Z_0^{(1)} K_x^{(1)}}{K_x^{(1)} - K_x^{(2)}}
\end{aligned}
\tag{2}
$$

Now the line whose equation is

$$
\begin{aligned}
X &= X_P \\
Z &= Z_P
\end{aligned}
$$

can be considered. It intersects the two homologous lines in two different points, whose *Y* coordinates are indicated with Y_1 and Y_2. Formally they are obtained by substituting the values (2) in equations #2 and #4 of (1):

$$
\begin{aligned}
Y_P^{(1)} &= Y_0^{(1)} + \frac{X_0^{(2)} - X_0^{(1)} - Z_0^{(2)} K_x^{(2)} + Z_0^{(2)} K_x^{(2)}}{K_x^{(1)} - K_x^{(2)}} K_y^{(1)} \\
Y_P^{(2)} &= Y_0^{(2)} + \frac{X_0^{(2)} - X_0^{(1)} + Z_0^{(2)} K_x^{(1)} - Z_0^{(2)} K_x^{(1)}}{K_x^{(1)} - K_x^{(2)}} K_y^{(2)}
\end{aligned}
\tag{3}
$$

These two values will coincide if the two considered lines exactly intersected and their difference can be used as a measure of their skewness. We define the quantity

$$
P_Y\ [\mathrm{m}] \coloneqq Y_P^{(2)} - Y_P^{(1)} \tag{4}
$$

as the *Y*-parallax in the object space, assuming that coordinates are measured in meters. To make it comparable with the usual parallax estimations, which are performed in the image space and are measured in microns, it is necessary to know the scale factor *n* of the images used. This allows calculation of the *y*-parallax in the image space:

$$
p_y\ [\mu\mathrm{m}] \coloneqq \frac{P_Y}{n}\, 10^6 \tag{5}
$$

These definitions fully satisfy the three requirements listed above. We investigated, in particular, item #3 by measuring the image coordinates of many points, calculating their parallaxes with (4), and asking the two operators who collaborated in the research to verify the correlation between our indicator and their visual observations. We came to the conclusion that (4) is an effective indicator of the perceived parallaxes.

5. Results for direct sensor estimation

Quality of the original EO values, obtained by direct sensor orientation, was investigated initially.

5.1. Residual parallaxes

Table 2 reports the main statistical parameters related to residual parallaxes for all the 21 standard models and for the whole block, in the last line. Columns respectively report: a progressive number, the names of the images constituting the model, the number of observed points, the number of observations, minimum and maximum parallaxes, maximum of the absolute value, mean, standard deviations and root mean square error of the parallaxes of each model; parallaxes are measured in microns. For the whole block, the number of observations is greater than the number of points, as many of them are visible in more than two images; the number of points indicated in the last line, 265, comes from the sum of the number of GCPs and pure tie points.

	image_1	image_2	points	obs	min	max	max(abs)	mean	std	rmse
1	**567**	**569**	**28**	**28**	**-57,74**	**4,10**	**57,74**	**-20,76**	**11,96**	**23,85**
2	815	817	25	25	-25,61	39,25	39,25	-11,84	11,94	16,65
3	**557**	**559**	**28**	**28**	**-38,29**	**-5,84**	**38,29**	**-22,66**	**6,62**	**23,57**
4	803	805	22	22	27,71	36,39	36,39	30,93	2,61	31,04
5	**649**	**651**	**28**	**28**	**-4,75**	**34,74**	**34,74**	**12,83**	**8,82**	**15,48**
6	653	655	27	27	12,84	34,58	34,58	20,02	4,69	20,54
7	645	647	29	29	-3,03	34,10	34,10	8,91	7,40	11,50
8	807	809	30	30	-32,25	5,00	32,25	-12,55	6,42	14,05
9	559	561	24	24	-6,95	31,87	31,87	18,45	7,14	19,73
10	**809**	**811**	**26**	**26**	**2,68**	**28,82**	**28,82**	**15,07**	**5,27**	**15,93**
11	563	565	24	24	-3,91	28,20	28,20	18,22	6,32	19,24
12	561	563	28	28	-11,87	27,30	27,30	6,14	8,90	10,68
13	569	571	26	26	-26,49	2,86	26,49	-11,19	6,98	13,12
14	647	649	26	26	-26,12	8,15	26,12	-8,28	8,49	11,75
15	811	813	28	28	-24,54	9,25	24,54	-8,55	6,06	10,42
16	805	807	26	26	-23,06	13,04	23,06	-1,98	6,09	6,29
17	813	815	23	23	9,24	22,42	22,42	15,10	3,59	15,51
18	565	567	23	23	-7,57	22,37	22,37	6,52	7,44	9,77
19	641	643	20	20	-21,08	11,56	21,08	3,63	7,41	8,08
20	651	653	25	25	-11,87	8,88	11,87	-3,62	5,70	6,66
21	643	645	25	25	-7,38	7,84	7,84	1,38	4,51	4,63
	Whole block		265	541	-57,74	39,25	57,74	2,05	15,87	15,99

Table 2 – Summary of residual parallaxes for each model and for the whole block. The four models which will be taken into account for further processing are displayed in red bold, in a boxed line.

Models are ordered with respect to the maximum of the absolute value, in decreasing order; lines which are red bold and boxed correspond to the four models which have been chosen as LPR dataset. They occupy the top part of the table; however their choice hasn't been driven by high parallax value only, but also by considering the availability of GCPs in the various models.

The definition of a sharp threshold such that parallax values which are above it disturb stereoscopic vision, is questionable. In our preliminary work, whose main goal was assessing correlation between calculated and perceived parallaxes, we noticed that the threshold can be fixed, for current block and images, at around 30 microns. Therefore, three of the four considered models are outliers, and one is on the borderline. For many other models, optimal stereovision is directly guaranteed by direct sensor orientation.

5.2. Accuracy

Table 3 reports the main statistical parameters related to the accuracy of stereoplotted coordinates, with respect to their true values, measured with GPS. These parameters are given in meters for the four chosen models and for the whole block.

Columns respectively report: the names of the images constituting the model, the number of observed points, the number of observations; then, for each component, X, Y, Z, maximum of the absolute value, mean, std and rmse of the residuals are given. The last line is about the whole block and again, in this case, the number of observations is greater than the number of points.

img_1	img_2	points	obs	X				Y				Z			
				max (abs)	mean	std	rmse	max (abs)	mean	std	rmse	max (abs)	mean	std	rmse
567	569	5	5	0,18	-0,15	0,03	0,15	0,32	-0,05	0,17	0,18	1,30	0,82	0,35	0,89
557	559	5	5	0,24	0,06	0,17	0,18	0,28	0,10	0,15	0,18	0,63	0,08	0,45	0,46
649	651	10	10	0,31	-0,24	0,05	0,24	0,37	0,00	0,17	0,17	0,84	0,55	0,26	0,61
809	811	8	8	0,29	0,06	0,11	0,13	0,32	-0,11	0,14	0,18	0,39	-0,15	0,15	0,21
Whole block		56	111	0,63	-0,07	0,18	0,19	0,55	-0,03	0,18	0,19	1,59	0,35	0,45	0,57

Table 3 - Summary of accuracy of stereoplotted coordinates in respect to GPS-measured ones.

Results are quite positive, even if a systematic error in height is detectable and should be investigated. However it must be underlined again that a detailed evaluation of the accuracy of the data is beyond the scope of this paper, as well as the elaboration of methods to improve it. Our research assumes that the accuracy guaranteed by direct sensor orientation is perfectly adequate for a certain scope and there is no need to augment it, and focuses on methods to reduce residual parallaxes and to improve quality of stereovision.

Therefore, quantities contained in Table 3 represent the accuracy's unsurpassable limit which is attainable with this EO data. The LPR procedure will be considered successful if it will significantly improve residual parallaxes, leaving accuracy unchanged or making it only a little worse because the general rule holds, that each data processing step increases numerical and random errors.

6. Finding the limits: relative orientation calculation

Table 3 shows the limits of the considered data in terms of accuracy. Before facing the LPR procedure, we established the potential of the LPR dataset in terms of parallaxes. We performed a sort of symmetric relative orientation. We started from the quantity

$$P_Y = Y_P^{(2)} - Y_P^{(1)} \qquad \text{(see (3) for definitions)} \tag{6}$$

considering it as a function of the EO parameters of both images, while image coordinates are treated as known. We solved the non linear least squares problem which minimizes the norm of the vector constituted by the parallaxes estimated on each of the tie points.

As it is well known, from relative orientation theory, that only 5 parameters can be estimated because of the invariance-indetermination nexus, we fixed $\boldsymbol{X}_0^{(1)}$, $\boldsymbol{X}_0^{(2)}$ and ω_1, as in traditional relative orientation, assigning them the original EO values, resulting from direct sensor orientation.

image_1	image_2	points	obs	min	max	max(abs)	mean	std	rmse
567	569	28	28	-18,12	14,97	18,12	0,04	6,97	6,97
557	559	28	28	-7,97	13,13	13,13	0,02	4,49	4,49
649	651	28	28	-13,46	16,59	16,59	0,04	6,09	6,09
809	811	26	26	-9,05	14,04	14,04	0,04	4,08	4,08

Table 4 – Summary of residual parallaxes for each model, after relative orientation.

As Table 4 shows, the images and the image coordinate measurements we performed have a potential quality, in terms of residual parallaxes, much greater than that shown by the original EO data, summarized by Table 2.

7. The LPR process

In this section the LPR process is described. We first explain the adjustment we use, from the mathematical point of view, then we show the results, highlighting their dependencies on the weights assigned to each observation.

7.1. The methodology

The LPR process is basically based on an AT adjustment, applied simply to a couple of images. The system of equations we solve contains, firstly, the usual AT observations based on the collinearity equations. But it is well known that the two-image block has no unique solution, because of the invariance-indetermination nexus. From the numerical point of view, this translates into the rank-deficiency of the matrix of the deterministic models.

Therefore we insert, as additional direct observations, the EO parameters of the images. Such parameters are among the unknowns of the problem, but we have measurement of them which we use, coming from direct sensor orientation. The **observation equations** are

$$x_{0i}^{(1)} = -c\frac{R_{11}^{(1)}\left(X_i - X_0^{(1)}\right) + R_{21}^{(1)}\left(Y_i - Y_0^{(1)}\right) + R_{31}^{(1)}\left(Z_i - Z_0^{(1)}\right)}{R_{13}^{(1)}\left(X_i - X_0^{(1)}\right) + R_{23}^{(1)}\left(Y_i - Y_0^{(1)}\right) + R_{33}^{(1)}\left(Z_i - Z_0^{(1)}\right)} \qquad i = 1,2,\ldots,n$$

$$y_{0i}^{(1)} = -c\frac{R_{12}^{(1)}\left(X_i - X_0^{(1)}\right) + R_{22}^{(1)}\left(Y_i - Y_0^{(1)}\right) + R_{32}^{(1)}\left(Z_i - Z_0^{(1)}\right)}{R_{13}^{(1)}\left(X_i - X_0^{(1)}\right) + R_{23}^{(1)}\left(Y_i - Y_0^{(1)}\right) + R_{33}^{(1)}\left(Z_i - Z_0^{(1)}\right)}$$

$$x_{0i}^{(2)} = -c\frac{R_{11}^{(2)}\left(X_i - X_0^{(2)}\right) + R_{21}^{(2)}\left(Y_i - Y_0^{(2)}\right) + R_{31}^{(2)}\left(Z_i - Z_0^{(2)}\right)}{R_{13}^{(2)}\left(X_i - X_0^{(2)}\right) + R_{23}^{(2)}\left(Y_i - Y_0^{(2)}\right) + R_{33}^{(2)}\left(Z_i - Z_0^{(2)}\right)}$$

$$y_{0i}^{(2)} = -c\frac{R_{12}^{(2)}\left(X_i - X_0^{(2)}\right) + R_{22}^{(2)}\left(Y_i - Y_0^{(2)}\right) + R_{32}^{(2)}\left(Z_i - Z_0^{(2)}\right)}{R_{13}^{(2)}\left(X_i - X_0^{(2)}\right) + R_{23}^{(2)}\left(Y_i - Y_0^{(2)}\right) + R_{33}^{(2)}\left(Z_i - Z_0^{(2)}\right)}$$

$$\omega_0^{(1)} = \omega^{(1)}$$
$$\varphi_0^{(1)} = \varphi^{(1)}$$
$$\kappa_0^{(1)} = \kappa^{(1)}$$
$$\omega_0^{(2)} = \omega^{(2)}$$
$$\varphi_0^{(2)} = \varphi^{(2)}$$
$$\kappa_0^{(2)} = \kappa^{(2)}$$

The **observations** are the image coordinates of each point on both images and the EO parameters of the images; the total number is $4n+12$ where n is the number of points. The **unknowns** are the object coordinates of the observed points and the EO parameters again; the total number is $3n+12$.

We do not use GCPs at all. If we have some, we use them as pure tie points, but we don't use, within the adjustment, the knowledge of their object coordinates: we use it during successive quality evaluation, instead.

When an adjustment with heterogeneous observations is performed, it is necessary to assign to each of them a **weight**. For EO, we used values given by Applanix, the manufacturer of the inertial integrates sensor:

$$\sigma_X = \sigma_Y = \sigma_Z = 0.05 \text{ m}$$
$$\sigma_\omega = \sigma_\varphi = 0.006 \text{ grad}$$
$$\sigma_\kappa = 0.009 \text{ grad}$$

For image coordinates, we started from Table 1

$$\sigma = \sigma_x = \sigma_y = 3 \text{ micron}$$

7.2. Results

Table 5 shows results of LPR when giving σ various values, from 3 to 27 micron. Using the true value for the accuracy of the image coordinates, 3 micron, LPR's results are very good for parallaxes, as they are similar to those of Table 4, coming from pure relative orientation, but they are very unsatisfactory for accuracy.

The explanation is that image coordinates and EO parameters given by direct sensor orientation can be thought as two different attractors, which are in disagreement. If the first one is too strong, it forces the final solution to move away from the second attractor, representing satisfactory values for accuracy.

σ (μm)	Img_1	Img_2	**Parallaxes** (μm)		**X** (m)		**Y** (m)		**Z** (m)	
			max(abs)	rmse	max(abs)	rmse	max(abs)	rmse	max(abs)	rmse
3	569	567	24,36	7,89	0,69	0,39	0,88	0,80	3,75	3,55
	559	557	12,86	5,21	0,19	0,16	0,58	0,43	2,66	2,03
	649	651	18,86	7,12	0,79	0,43	1,03	0,57	3,43	3,00
	809	811	14,41	4,67	0,24	0,12	0,43	0,28	1,31	1,13
9	569	567	28,69	9,36	0,21	0,14	0,32	0,27	1,47	1,33
	559	557	15,33	6,17	0,21	0,16	0,21	0,17	1,07	0,65
	649	651	20,50	8,31	0,36	0,24	0,52	0,22	1,40	1,02
	809	811	14,69	5,23	0,25	0,11	0,30	0,16	0,27	0,17
15	569	567	30,50	9,98	0,17	0,14	0,28	0,20	1,20	1,03
	559	557	15,46	6,41	0,24	0,18	0,26	0,18	0,84	0,54
	649	651	21,31	8,53	0,30	0,24	0,44	0,19	1,11	0,77
	809	811	14,98	5,33	0,28	0,12	0,31	0,17	0,28	0,16
21	569	567	33,20	10,53	0,16	0,14	0,28	0,18	1,19	0,95
	559	557	15,21	6,61	0,25	0,18	0,27	0,19	0,76	0,51
	649	651	22,03	8,65	0,31	0,24	0,42	0,18	1,01	0,70
	809	811	15,40	5,43	0,29	0,12	0,31	0,18	0,33	0,18
27	569	567	35,37	11,03	0,16	0,14	0,29	0,18	1,20	0,92
	559	557	15,95	6,88	0,25	0,18	0,28	0,19	0,72	0,49
	649	651	22,72	8,77	0,31	0,24	0,40	0,17	0,96	0,67
	809	811	15,92	5,57	0,29	0,12	0,32	0,18	0,35	0,19

Table 5 – Summary of residual parallaxes and accuracies for each model, after LPR with various values of σ.

Figure 2 summarizes the behavior of LPR as a function of σ, for the model 567-569, which is the most difficult one: as σ increases, residual parallaxes increase and accuracy improves. A good compromise is probably represented by the choice σ=15 μm, approximately corresponding to the pixel size. In this case parallaxes are all within the previously fixed limit of 30 microns and rmse passes from 24 to 10 microns. At the same time, accuracies do not exceed 110% of the original ones.

In Figure 2 the behavior of rmse of parallaxes and of residuals of object coordinates of GCPs are shown. The figure shows the dramatic gain assured by LPR, in terms of parallaxes and also the convergence of accuracies towards satisfactory values. Dotted lines represent lower and upper limits. For parallaxes, the blue dotted line represents results obtained from direct sensor orientation EO data, while the green dotted line represents results from relative orientation. For accuracies, each continuous line, which represents accuracy of LPR, has a corresponding dotted line, representing the accuracy attainable with the original EO data, which is regarded as the optimal value.

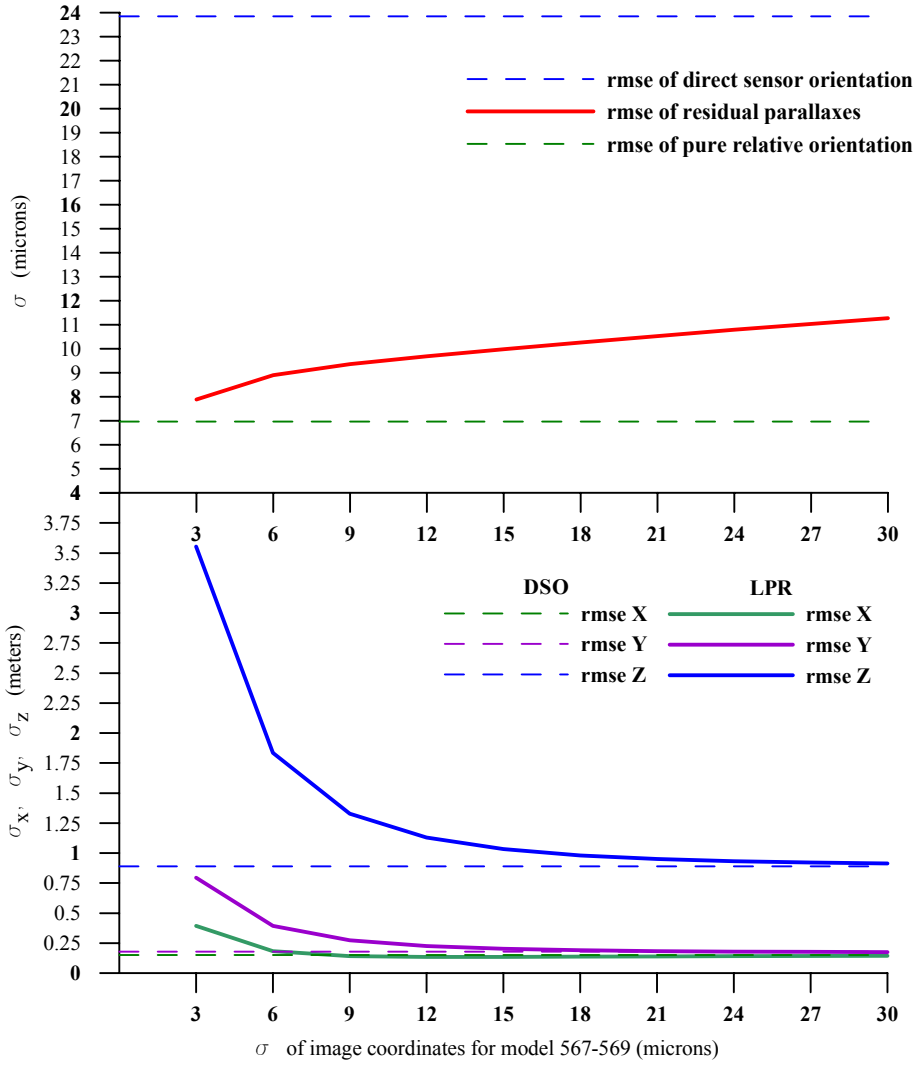

Figure 2 – LPR results, as a function of σ.

8. Conclusions and perspectives

A method for improving stereovision of directly oriented images has been described and tested. It doesn't require any additional data; it is capable of a significant reduction of residual parallaxes and, at the same time, it leaves accuracies almost unchanged: results are completely satisfactory. Before considering the method fully tested, we need to apply it to a greater number of models and also to other blocks.

A procedure which is adaptive and capable of giving full quality feedback is under development. In its current development, LPR requires, for tuning the weights, the availability of GCPs and they are also necessary for accuracy assessment. The augmented version of LPR will take advantage of the difference between the object coordinates of tie points determined exploiting direct measured EO values, $\mathbf{X}_{DSO}$, ant those obtained by LPR-optimized EO values, $\mathbf{X}_{LPR}$.

Other methodologies will also be taken into consideration. One is based on the successive calculation of relative and absolute orientation. The first step will create the stereomodel, as well as is possible, while the second will match the model reference system onto the object one. The latter pass presents some new aspects because the absolute orientation calculation is usually a match between two sets of coordinates, while in this case it will be a match between two sets of EO parameters.

9. Acknowledgments

The research presented in this paper was carried out in the frame of the National Research Project entitled *Integrated inertial positioning systems in aerial Photogrammetry*, co-funded by the Italian Ministry of the University for the year 2002, and chaired by prof. Galetto of the University of Pavia.

10. Bibliography

[1] Casella, V., Galetto, R., Surace, L., Ferretti, L., Banchini, G., Cavalli, A., 2001. Esperienze di fotogrammetria supportate da GPS/INS. Bollettino SIFET, n. 4, pagg. 35-49, ISSN 0392-4424, Parma.

[2] Colomina, I., 2002. Modern sensor orientation technologies and procedures. Test Report and Workshop Proceedings, Official Publication n°43, pagg. 59-70, Bundesamt für Kartographie und Geodäsie, Frankfurt am Main.

[3] Cramer, M., Stallmann, D., Haala, N., 2000. Direct georeferencing using GPS/INS exterior orientation for photogrammetric applications. Proceedings of XIXth ISPRS Congress, vol. 33, part B3/1, pagg. 198-205, Amsterdam.

[4] Cramer, M.,2001. On the use of direct georeferencing in airborne photogrammetry. Proceedings of IIIrd International Symposium on Mobile Mapping Technology, Cairo.

[5] Forlani, G., Pinto, L., 2001. Integrated INS/DGPS systems: calibration and combined block adjustment. OEEPE Workshop "Integrated Sensor Orientation", Institut für Photogrammetrie und GeoInformation, Universität Hannover, Heidelberg, Germany.

[6] Galetto, R., Casella, V., 2003. An Italian national research project on inertial positioning in photogrammetry. ISPRS International Workshop, WG I/5, Barcelona.

[7] Kraus, K., 1994. Fotogrammetria. Libreria Universitaria Levrotto & Bella, Torino.

[8] Habib, A., Schenk, T., 2001. Accuracy analysis of reconstructed points in object space from direct and indirect exterior orientation methods. OEEPE Workshop "Integrated Sensor Orientation", Institut für Photogrammetrie und GeoInformation, Universität Hannover, Heidelberg, Germany.

[9] Heipke, C., Jacobsen, K., Wegmann, H., 2001. The OEEPE test on integrated sensor orientation - results of phase 1. Fritsch/Spiller Eds, Wichmann Verlag.

[10] Heipke, C., Jacobsen, K., Wegmann, H., 2002. Analysis of the results of the OEEPE test “Integrated Sensor Orientation”. Test Report and Workshop Proceedings, Official Publication n°43, pagg. 31-45, Bundesamt für Kartographie und Geodäsie, Frankfurt am Main.

[11] Jacobsen, K., Wegmann, H., 2002. Dependencies and problems of Direct Sensor Orientation. Test Report and Workshop Proceedings, Official Publication n°43, pagg. 73-84, Bundesamt für Kartographie und Geodäsie, Frankfurt am Main.

[12] Jacobsen, K., 2000. Potential and limitation of Direct Sensor Orientation. Proceedings of XIXth Congress of ISPRS, vol. 33, part B3/1, pagg. 423-429, Amsterdam.